Dynamics and Lattice-Size Dependence of Surface Mean Slope in Thin-Film Deposition

Jianqiao Huang,[†] Gangshi Hu,[†] Gerassimos Orkoulas,[†] and Panagiotis D. Christofides*[,†,‡]

Department of Chemical and Biomolecular Engineering and Department of Electrical Engineering, University of California, Los Angeles, California 90095

This work focuses on the study of the dynamic behavior and lattice-size dependence of the surface root-mean-square slope of thin-film deposition processes that involve thermal balance between film growth and surface relaxation. Two different deposition processes taking place on square and triangular lattices are introduced and used to investigate the dynamics and lattice-size dependence of the surface root-mean-square slope. The simulation results indicate that the expected mean slope square reaches quickly a steady-state value and exhibits a very weak dependence with respect to lattice size variation. The simulation findings are corroborated by an analysis of appropriate finite-difference discretizations of surface height profiles computed by an Edwards−Wilkinson-type partial differential equation that can be used to describe the dynamics of surface height profile in the deposition processes under consideration.

1. Introduction

Photovoltaic cells (solar cells) constitute an important source of sustainable energy, which directly utilizes solar energy. However, the limited conversion efficiency of the solar power prevents the wide application of solar cells. Thin-film silicon solar cells are currently the most developed and widely used solar cells.[1] Research on optical and electrical modeling of thin-film silicon solar cells indicates that the scattering properties of the thin-film interfaces are directly related to the light trapping process and the efficiencies of thin-film silicon solar cells.[2,3] For example, a higher diffused transmittance of incident light is desired for the upper surface of solar cells for a maximum energy input. The scattering properties of the interfaces are characterized by the surface morphology, which includes root-mean-square (rms) roughness and rms slope.[4] It is desired to improve the conversion efficiency of thin-film solar cells via the regulation of surface morphology of thin-film solar cells during the manufacturing process, i.e., thin-film deposition process, by appropriately tailoring the surface rms slope and rms roughness to desired specifications.

Kinetic Monte Carlo (kMC) methods have been widely used to simulate thin-film microscopic processes by utilizing microscopic film growth processes and kinetics that are obtained from molecular dynamics simulations and experiments.[5−8] KMC lattice models based on a solid-on-solid (SOS) assumption were initially developed, in which particles land on top of film particles. However, the SOS models can only simulate the growth of dense thin-films and are inadequate in capturing the evolution of thin-film porosity, which has emerged as an important film quality variable that strongly influences the electrical and mechanical properties of semiconductor devices. To overcome this limitation, triangular-lattice-based kMC models have been developed that allow overhangs and vacancies to develop inside the film.[6−9] The dependence of the surface roughness and porosity of kMC models of porous thin-film deposition processes on lattice size and operating conditions were recently investigated.[10] Due to their ability to simulate thin-film growth processes, kMC models have also been used in the context of feedback control of thin-film surface roughness.[11,12]

However, kMC models have several disadvantages that prevent them from being widely used in the feedback control design. First, the computational cost that kMC simulations require is high for real-time monitoring and control purposes. Second, the kMC models are not available in closed form, and thus, they cannot be used to design model-based feedback control systems and perform system-level analysis. Alternatively, stochastic differential equation (SDE) models were introduced to model surface morphology in a variety of thin-film preparation processes.[13,14] SDE models can be derived from the corresponding master equations of the microscopic processes or identified from the available simulation data or experimental data. SDE models have been successfully used to describe the evolutions of surface height profiles and surface roughness.[10] Furthermore, methodologies have been developed to construct SDE models and estimate their parameters from first principles[15−17] and numerical simulations.[18] Recently, control of thin-film microstructure using SDE models has attracted significant attention.[19−22] However, the dynamics and control of the rms slope of surface height profiles in thin-film deposition processes has not been studied.

Motivated by these considerations, this work focuses on the study of the dynamic behavior and lattice size dependence of the surface root-mean-square slope of thin-film deposition processes. Two different deposition processes are investigated: a random deposition with surface relaxation process and a porous thin-film deposition process. Both deposition processes involve a deposition (adsorption) process and a relaxation (migration) process, which strongly influence the resulting thin-film surface morphology. KMC methods are used to simulate the deposition processes and generate film surface height profiles and compute rms slope and roughness. The simulation results indicate that the expected mean slope square reaches quickly a steady-state value and exhibits a very weak dependence with respect to lattice size variation. A theoretical analysis is provided using an Edwards−Wilkinson (EW) type partial differential equation (PDE) that can describe the dynamics of the surface height profile in the deposition processes under consideration. The kMC simulation findings are corroborated by the analytical

* To whom correspondence should be addressed. E-mail: pdc@seas.ucla.edu. Phone: +1 (310) 794-1015. Fax: +1 (310) 206-4107.
[†] Department of Chemical and Biomolecular Engineering.
[‡] Department of Electrical Engineering.

10.1021/ie100012w
Published on Web 05/21/2010

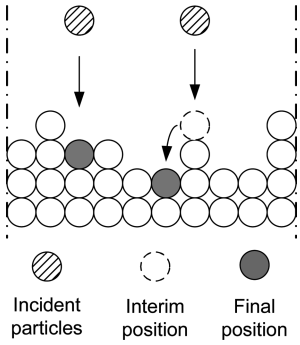

Figure 1. Random deposition process with surface relaxation and examples of deposition and surface relaxation processes. A square lattice is used.

results of appropriate finite-difference discretizations of the solutions of the EW equation model.

2. Thin-Film Deposition Processes

In this section, two thin-film deposition processes are considered and modeled by using on-lattice kMC models. The first process is a random deposition process with surface relaxation taking place on a square lattice where solid-on-solid (SOS) assumption is made.[23] The second process is a porous thin-film deposition process taking place on a triangular lattice where vacancies and overhangs are allowed to develop.[10,22] Periodic boundary conditions (PBCs) are applied to both lattice models. In both deposition processes, there are two competing effects which influence the evolution of the surface height profiles: a growth effect and a relaxation effect. The definitions of surface height profile and root-mean-square slope are also introduced.

2.1. Random Deposition with Surface Relaxation Process Model. The random deposition process with surface relaxation is modeled on a one-dimensional in the lateral direction square lattice with SOS assumption, where particles land on top of the existing surface particles. The lattice size in this model denotes the number of sites. The deposition rate is denoted by W and has the unit of deposited layers per second. Figure 1 shows the lattice model of the random deposition process with surface relaxation and examples of the deposition processes.

When a particle is deposited, a site is first randomly chosen among all lattice sites. After the site is determined, an incident particle deposits on the top of the highest particle on that site. Upon deposition, a surface relaxation process takes places if the height of the deposited site (before the deposition process) is higher in the growth direction than the height of any of the two adjacent sites. When the surface relaxation process is conducted, the incident particle relaxes to the lowest site among its two nearest neighboring sites. If both neighboring sites have lower heights, the incident particle randomly chooses (with equal probability) a neighboring site as its final deposition site.

2.2. Porous Thin-Film Deposition Process Model. Figure 2 shows the porous thin-film growth process taking place on a one-dimensional in the lateral direction triangular lattice. In this lattice model, the lattice size denotes the number of sites in the lateral direction per layer, i.e., the maximum number of particles that can be packed within one horizontal layer. The coordination number of the triangular lattice is six, so a particle on the lattice can have at most six nearest neighbors. In the bottom of the lattice, a fully packed and fixed substrate layer is initially placed and is used to initiate the thin-film deposition process.

We consider two different types of microprocesses taking place in this deposition process: an adsorption process and a migration process. In the adsorption process, incident particles are deposited from the gas phase and are incorporated into the thin-film. In this work, only vertical incidence is considered in the adsorption process. When an incident particle is incorporated into the film, it moves to the nearest vacant site of the contacting particle. If the incident particle moves to a site that has only one nearest neighbor, it is considered to be an unstable particle in the lattice and relaxes instantaneously to the most stable vacant site neighboring the unstable site, i.e., the site that has the most nearest neighbors.

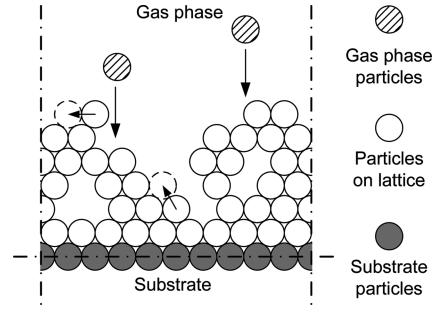

Figure 2. Thin-film growth process on a triangular lattice. The arrows denote adsorption and migration processes.

In a migration process, particles on the thin-film overcome the energy barrier of their sites and move to their adjacent vacant sites.[9,24] Substrate particles cannot move. The migration rate follows an Arrhenius-type law, where the pre-exponential factor and the activation energy are taken from a silicon film [see ref 10 for details].

The microstructure of the porous thin-film is the result of a complex interplay between adsorption and migration processes. The macroscopic operating variables of the deposition process influence the resulting film microstructure. The two variables that are considered in this process are the adsorption rate and the substrate temperature. The adsorption rate, which is denoted by W, is defined as the number of deposited layers per second. The substrate temperature, which is denoted by T, has a strong influence on the migration rate via the Arrhenius rate law.

In this work, the microscopic rules are used in kMC methods to simulate both the random deposition with surface relaxation process and the porous thin-film deposition process. Specifically, a continuous-time Monte Carlo (CTMC) type method (e.g., ref 25) is used to carry out the kMC simulations.

2.3. Definition of Variables. In this section, the variables that characterize the film surface morphology are defined. Surface height profile represents the film surface morphology and is defined as the connection of the centers of the surface particles. For the porous thin-film deposition process, surface particles are determined as the particles that can be reached from above in the vertical direction without being fully blocked by other particles on the film.[10,22] Figure 3 shows an example of the surface height profile of the porous thin-film deposition process. For the random deposition process with surface relaxation, the surface particles can be easily identified as the top particles on all lattice sites due to the SOS assumption.

Surface roughness is a commonly used measure of thin-film surface morphology and is defined as the root-mean-square (rms) of surface height profile as follows:

$$r = \left[\frac{1}{n_L}\sum_{i=1}^{n_L}(h_i - \bar{h})^2\right]^{1/2} \quad (1)$$

where r denotes surface roughness, h_i, $i = 1, 2, ..., n_L$, is the surface height at the ith position in the unit of layer, and $\bar{h} =$

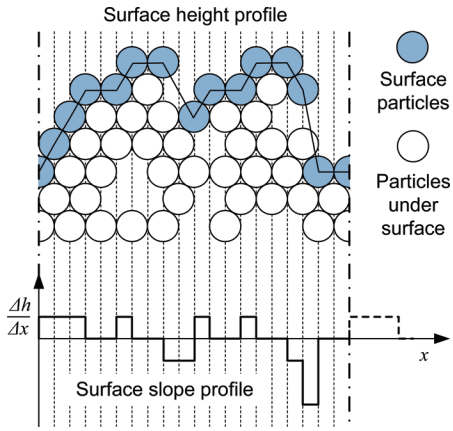

Figure 3. Example showing the definition of the surface height profile and the calculation of the corresponding surface slope profile.

$(1/n_L)\sum_{i=1}^{n_L} h_i$ is the average surface height. We note that the number of height positions in eq 1, n_L, does not always equal the lattice size, L. In the porous thin-film deposition process, the number of height positions equals $2L$ due to the nature of the triangular lattice in the porous thin-film deposition process; see Figure 3 for example. For the random deposition process with surface relaxation, n_L is simply L due to the use of a square lattice.

In addition to surface roughness, the gradient (slope) of surface height profile is another important variable that determines the surface morphology. In this work, the root-mean-square (rms) slope represents the extent of surface slope and is defined in a similar fashion to surface roughness as follows:

$$m = \left[\frac{k_m^{\,2}}{n_L}\sum_{i=1}^{n_L}(h_{i+1} - h_i)^2\right]^{1/2} \qquad (2)$$

where m denotes the rms slope, which is a dimensionless variable, and k_m denotes the geometric ratio between the single-layer height and the interval between adjacent height positions. Due to the use of PBCs, the slope at the last position ($i = n_L$) is computed as the surface height difference between the last lattice site and the first lattice site. The value of the geometric ratio in eq 2, k_m, is 1 for the random deposition process with surface relaxation and $\sqrt{3}$ for the porous thin-film deposition process. Figure 3 shows an example of the surface slope obtained from the surface height profile in the porous thin-film deposition process.

The two variables that are related to the surface morphology, surface roughness, and rms slope, are defined in a similar fashion, i.e., root mean squares of a spatial profile. However, surface roughness is calculated on the basis of surface height profile, while rms slope is based on the surface slope profile. Thus, the two variables describe different properties of the surface height profile. Surface roughness measures the correlation of surface height at all sites with the average height, and thus, the sequence of the surface sites does not affect the calculation of surface roughness. On the contrary, surface slope is the height difference between two adjacent surface sites. As a result, rms slope measures the height correlation of adjacent surface sites and is sensitive to the sequence of surface sites. Therefore, two surface profiles with the same roughness may have very different rms slope profiles. We also note that surface roughness and rms slope are not fully independent. In the extreme case of a flat surface, surface roughness and rms slope both have zero values.

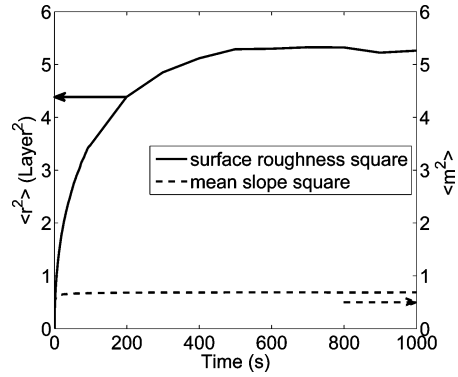

Figure 4. Profiles of the expected mean slope square (dashed line) and surface roughness square (solid line) from kMC simulations with lattice size $L = 100$; random deposition process with surface relaxation with $W =$ 1 layer/s.

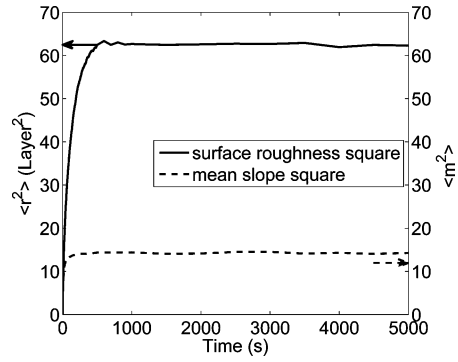

Figure 5. Profiles of the expected mean slope square (dashed line) and surface roughness square (solid line) from kMC simulations with lattice size $L = 100$; porous thin-film deposition process with $W = 1$ layer/s and $T = 300$ K.

3. Rms Slope Behavior

In this section, the rms slope is calculated from the surface height profiles of the two deposition processes. The behavior of rms slope, i.e., its dynamics and dependence on lattice size, is then investigated. For the convenience of theoretical analysis and comparison with the simulations, the square of rms slope (mean slope square), i.e., m^2, is used to present the results.

3.1. Dynamics of rms Slope. To investigate the dynamics of rms slope, kMC simulations of the two deposition processes are carried out with fixed operating conditions throughout the entire simulation. The lattice size is fixed to 100 sites for both processes for the results to be presented in this section. The simulation duration is large enough to allow the rms slope to reach its steady-state value. Due to the stochastic nature of kMC methods, different simulation runs may result in different lattice configurations and different surface morphology. Multiple independent simulations runs (10 000−25 000 runs) are carried out to generate smooth profiles of statistical moments, i.e., expected values and variances.

Figures 4 and 5 show the profiles of the expected mean slope square. The operating conditions are fixed at a substrate temperature of 300 K (in the porous thin-film deposition process) and an adsorption rate of 1 layer/s (in both deposition processes). Figures 4 and 5 also include the profiles of the corresponding expected roughness square. In both figures, the mean slope square profiles evolve similarly to the roughness square profiles: mean slope square increases from zero and approaches a finite steady-state value at large times.

However, it can be seen from Figures 4 and 5 that the dynamics of roughness square and mean slope square are

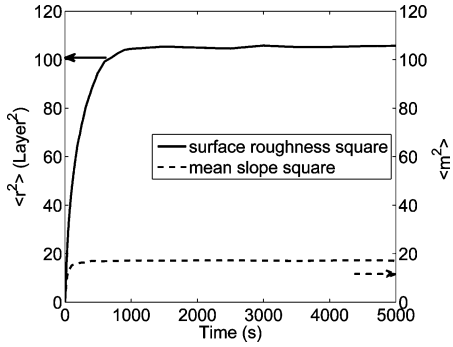

Figure 6. Profiles of the expected mean slope square (dashed line) and surface roughness square (solid line) from kMC simulations with lattice size $L = 100$; porous thin-film deposition process with $W = 1$ layer/s and $T = 500$ K.

different in many aspects. First, the mean slope square has faster dynamics than roughness square. Here, the dynamics of a profile refer to the steady-state time, t_{ss}, that is needed for the profile to reach the steady-state value (practically, we take 99% of the steady-state value as the threshold to calculate t_{ss}). In general, a smaller steady-state time indicates faster dynamics. Specifically, in the random deposition with surface relaxation process of Figure 4, $t_{ss} \simeq 125$ s for slope and $t_{ss} \simeq 469$ s for roughness; in the porous thin-film deposition process of Figure 5, for $T = 300$ K, $t_{ss} \simeq 190$ s for slope and $t_{ss} \simeq 467$ s for roughness. Second, the steady-state values of mean slope square are smaller than the steady-state values of roughness square (even taking into consideration the geometric ratios). These differences can be explained as follows: the height correlation of adjacent surface sites, which mean slope square measures, is higher than the surface height correlation with the average height which is measured by the surface roughness. The higher correlation results in a smaller difference, i.e., a smaller steady-state value, and faster dynamics of mean slope square than surface roughness.

3.2. Dependence of rms Slope on Operating Conditions. The dynamics of rms slope depend on operating conditions and lattice size. KMC simulations are also carried out to find out the dependence of rms slope with respect to different operating conditions. For the random deposition with surface relaxation process, the dynamics of the entire process scales proportionally with the adsorption rate, i.e., the higher the adsorption rate, the faster the rms slope and rms roughness approach their steady state values. However, the dynamics of the porous thin-film deposition process have a complex dependence on the operating conditions, i.e., substrate temperature or adsorption rate below.

Figure 6 shows the profile of the expected mean slope square and roughness square of the porous thin-film deposition process at a substrate temperature of $T = 500$ K; the adsorption rate is kept at $W = 1$ layer/s. From the comparison between Figures 5 and 6, it is evident that both the rms slope and the surface roughness increase as the substrate temperature increases from 300 to 500 K. These consistent results indicate that the rms slope and surface roughness can be captured by the same analytical dynamic equation, as we will discuss in section 4.

Figure 7 shows the profiles of the expected mean slope square at different substrate temperatures. The adsorption rate is kept at $W = 1$ layer/s. A lattice size of 100 sites is used in all simulations for a meaningful comparison. It can be clearly seen from Figure 7 that the substrate temperature has a strong influence on the evolution of the rms slope. At low temperatures ($T \leq 400$ K), the particles have limited mobility, and thus, the evolution profiles of the mean slope square are nearly insensitive

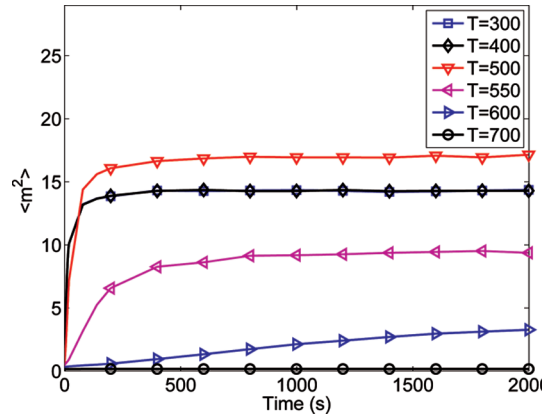

Figure 7. Profiles of the expected mean slope square from kMC simulations at different substrate temperatures; porous thin-film deposition process with $W = 1$ layer/s and $L = 100$.

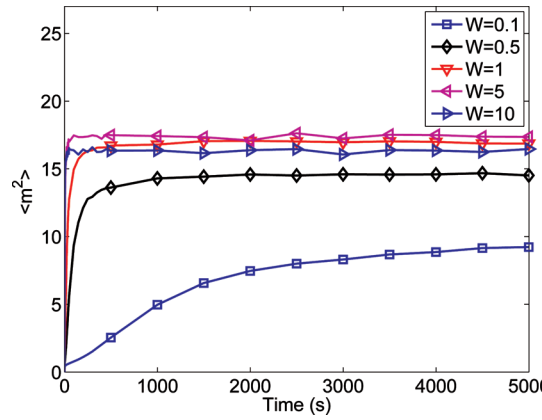

Figure 8. Profiles of the expected mean slope square from kMC simulations at different adsorption rates; porous thin-film deposition process with $T = 500$ K and $L = 100$.

to temperature variation. As temperature increases, however, the mean slope square profiles have higher values. At high temperatures ($T \geq 700$ K), the intensive mobility of particles results in an almost flat surface and the mean slope square is close to zero.

A similar dependence of the expected mean slope square on adsorption rate can be found in Figure 8, which shows the profiles of the expected mean slope square at different adsorption rates with a fixed substrate temperature of $T = 500$ K. The thin-film morphology is determined by the thermal balance between the adsorption process and the migration process. Thus, the expected mean slope square under a high adsorption rate behaves similarly to the one under a low substrate temperature (equivalently a low migration rate) and vice versa. This strong dependence on operating conditions can be used to design feedback controllers that regulate the rms slope of the thin-film surface at desired values that optimize thin-film reflectance and transmittance.

3.3. Lattice-Size Dependence of rms Slope. In this subsection, the lattice-size dependence of rms slope is studied for both deposition processes. To investigate the dependence of rms slope on lattice size, kMC simulations of the deposition processes are carried out for different lattice sizes (from 20 to 500). The operating conditions are fixed at $T = 300$ K and $W = 1$ layer/s for all simulations where applicable. Both evolution profiles and steady-state dependence of the expected mean slope square are presented. In the figures of steady-state dependence, the error

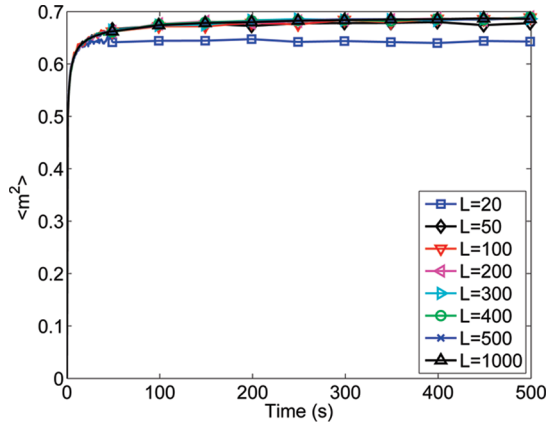

Figure 9. Profiles of the expected mean slope square from kMC simulations with different lattice sizes; random deposition process with surface relaxation with $W = 1$ layer/s.

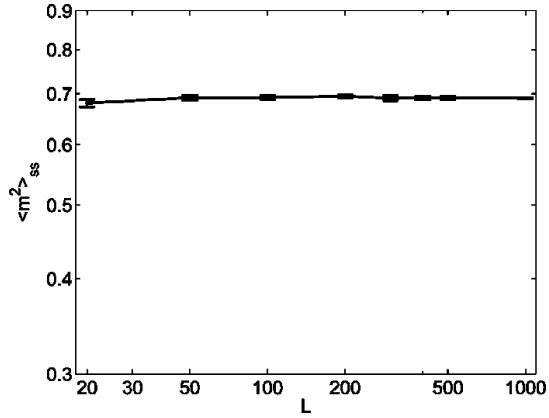

Figure 10. Dependence of the steady-state values of the expected mean slope square with error bars from kMC simulations, on the lattice size, L; random deposition process with surface relaxation with $W = 1$ layer/s.

bars are calculated from 20 averages of evenly divided groups of all simulation runs.

Figure 9 shows the profiles of the expected mean slope square of the random deposition with surface relaxation process for different lattice sizes. From Figure 9, it can be seen that the dynamics of mean slope square have a weak relationship with the lattice size at large lattice sizes, i.e., the profiles of mean slope square evolve and reach their steady states at similar time instants regardless of the lattice size. Similar to the dynamics, the steady-state values of mean slope square also have a weak dependence on lattice size, especially at large lattice sizes. This dependence of steady-state values on lattice size is different from the scaling properties of the surface roughness,[26] i.e., the lattice-size dependence of mean slope square does not follow a power law. The weak dependence can be observed more clearly in Figure 10, which shows the steady-state values of the expected mean slope square for different lattice sizes in a log−log plot. Similar evolution profiles and lattice-size dependence can be seen for the porous thin-film deposition process at different operating conditions; see Figures 11 and 12 for $T = 300$ K and Figures 13 and 14 for $T = 500$ K (the deposition rate is 1 layer/s for both cases).

In previous work, a linear lattice-size dependence of the steady-state value of expected surface roughness square was found.[10] In the next section, analytical and numerical results will be obtained and discussed from a stochastic PDE model of the thin-film deposition processes under consideration to explain the behavior of the expected mean slope square.

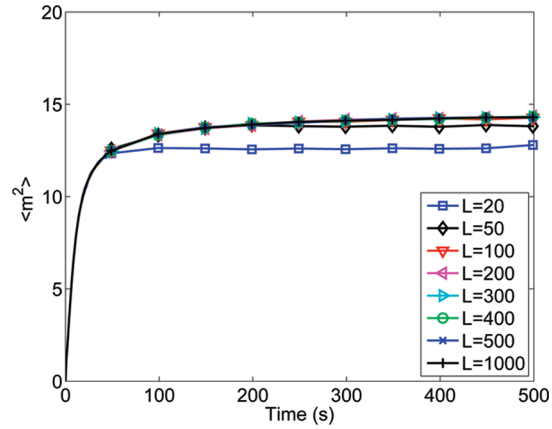

Figure 11. Profiles of the expected mean slope square from kMC simulations for different lattice sizes; porous thin-film deposition process with $W = 1$ layer/s and $T = 300$ K.

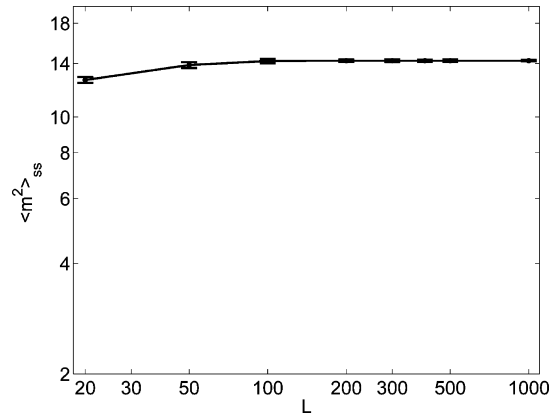

Figure 12. Dependence of the steady-state values of the expected mean slope square with error bars from kMC simulations, on the lattice size, L; porous thin-film deposition process with $W = 1$ layer/s and $T = 300$ K.

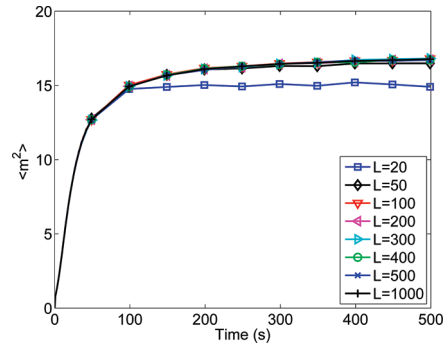

Figure 13. Profiles of the expected mean slope square from kMC simulations for different lattice sizes; porous thin-film deposition process with $W = 1$ layer/s and $T = 500$ K.

Remark 1. *For atomic depositions, the length scale of the crystalline lattice (0.5 nm) is smaller than the scale of the wavelength of the visible light (400−700 nm). Thus, the surface irregularity at the atom/molecular level cannot be related to the optical property of thin films. To be able to simulate a realistic domain size, we would need to have a lattice size of the order of 10^6 (with each site corresponding to atomic dimension) or higher, which is beyond the currently available computing power. If this simulation were possible, we would look at subdomains of the lattice of dimension of the order 400−700 nm and estimate an overall subdomain slope that the light "sees". In this setup, the overall slope of a given*

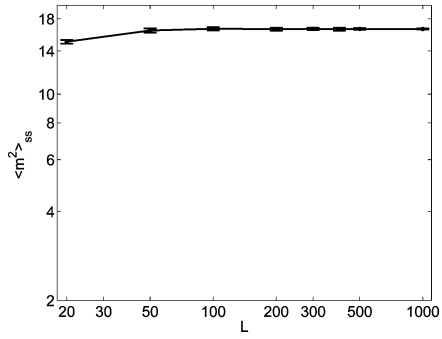

Figure 14. Dependence of the steady-state values of the expected mean slope square with error bars from kMC simulations, on the lattice size, L; porous thin-film deposition process with $W = 1$ layer/s and $T = 500$ K.

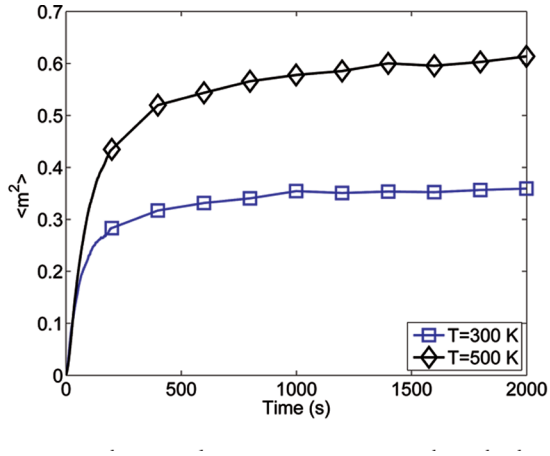

Figure 15. Profiles of the expected mean slope square computed on the basis of the average heights of groups of 10 surface particles from kMC simulations with $L = 1000$ at $T = 300$ K and 500 K; porous thin-film deposition process with $W = 1$ layer/s.

subdomain could be computed in an approximate way by computing average heights of groups of sites embedded in the subdomain and then connecting these average heights to compute the overall slope of the subdomain. We have applied this approach to the maximum order of domain size that we can simulate with our current computing power, L = 1000, and have computed average heights of groups of 10 sites and the corresponding m profile. Figure 15 shows the resulting m profile; we can see that the fast dynamics and approach of m to a finite steady-state value that we observe for the small lattice-size problem (L = 100 and m defined between adjacent heights as done in our work) from Figures 5 and 6 are also observed in this larger scale problem. Therefore, the metric m we have used for L = 100 gives us some insight into the behavior of a more complex problem that cannot be currently simulated.

Remark 2. *We note that, in the triangular lattice in the porous thin-film growth process, particles are only stable with two or more nearest neighbors, and thus, the typical height difference between adjacent lattice sites is zero or one layer. However, it can be inferred on the basis of the steady-state values in Figures 12 and 14 that an average vertical height difference between adjacent lattice sites is between 2 and 3 layers. This difference is significantly higher than the typical value, which is less than one layer. Such a large height difference between adjacent lattice size is the result of the columnar growth film structure in the low temperature region (T = 300−500 K); as can be seen in Figure 16, which shows that the surface height profile of the thin-film with a columnar*

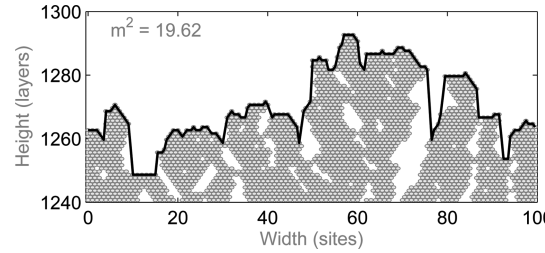

Figure 16. Snapshot of the film surface morphology at steady state (t = 1000s); porous thin-film deposition process with $T = 500$ K and $W = 1.0$ layer/s.

structure formed at T = 500 K contains steep "cliffs" (large differences between few adjacent surface height positions). These large height differences, although very few, contribute significantly to the root-mean-square value of the vertical height difference, i.e., 2 or 3 in the porous thin film growth process at T = 300 and 500 K.

4. Analytical and Numerical Results from the Stochastic PDE Model

The thin-film deposition is a stochastic process, where fluctuations are intrinsic and should be considered in the dynamic equation that describes the dynamics of the process. However, the surface irregularities of the thin-film are not purely random; otherwise, the surface roughness square and the mean slope square cannot reach their respective steady states but rather increase (linearly) to infinity as time increases.

To this end, an Edwards−Wilkinson-type equation with appropriately fitted parameters, which is a second-order stochastic PDE, is used to describe the dynamics and evolution of the surface height profile of the random deposition with surface relaxation process and the porous thin-film growth process.[10,13,27,28]

Furthermore, due to the fact that stochastic PDEs are defined on a continuous spatial domain, the dynamics of the rms slope obtained from the EW equation are different from the kMC simulations on the discrete lattice, i.e., an infinite value of mean slope square and a reciprocal dependence on the domain size are obtained from the continuum EW equation (see also remark 3 for more discussion on this issue). This inconsistency of the dynamics of the rms slope originates from the discretization of a continuous domain. Consistent numerical results to the ones of the kMC simulation are obtained from the discretization of the solution of the EW equation. This corroboration further supports the use of the EW equation as a continuum model to describe the evolution of surface height profile and the dynamics of the rms slope in the deposition processes considered in this work.

In the EW formalism, $h(x, t)$ represents the surface height profile in the continuum spatial domain case and the equation takes the following form:[10,13]

$$\frac{\partial h}{\partial t} = r_h + \nu \frac{\partial^2 h}{\partial x^2} + \xi(x,t) \tag{3}$$

subject to the following PBCs

$$h(-L_0, t) = h(L_0, t), \qquad \frac{\partial h}{\partial x}(-L_0, t) = \frac{\partial h}{\partial x}(L_0, t) \tag{4}$$

and the initial condition:

$$h(x, 0) = h_0(x) \tag{5}$$

where $x \in [-L_0, L_0]$ is the spatial coordinate, t is the time, and $\xi(x, t)$ is a Gaussian white noise with the following expressions for its mean and covariance:

$$\begin{aligned} \langle \xi(x,t) \rangle &= 0 \\ \langle \xi(x,t)\xi(x',t') \rangle &= \sigma^2 \delta(x - x')\delta(t - t') \end{aligned} \tag{6}$$

where $\langle \cdot \rangle$ denotes the mean value, σ^2 is a parameter which measures the intensity of the Gaussian white noise, and $\delta(\cdot)$ denotes the standard Dirac delta function.

In the EW equation of eq 3, r_h, ν, and σ^2 are model parameters. Specifically, r_h is related to the growth of average surface height, ν is related to the effect of surface particle relaxation and migration, and σ^2 is related to the noise intensity. Since r_h is only related to the averaged surface height, this term can be ignored for the purpose of studying the dynamics and scaling behavior of surface roughness and rms slope, i.e., $r_h = 0$.[10]

4.1. Analytical Derivation. The behavior of surface roughness can be derived from the EW equation of eq 3. Specifically, the steady-state value of the expected surface roughness square scales linearly with the domain size. This lattice-size dependence of surface roughness is consistent with the kMC simulation results of the porous thin-film deposition process as well as of other processes.[10]

The dynamics of rms slope can be derived from the EW equation using modal decomposition. A direct computation of the following eigenvalue problem of the linear operator of eq 3 subject to the PBCs of eq 4,

$$\begin{aligned} \nu \frac{\mathrm{d}^2 \bar{\phi}_n(x)}{\mathrm{d}x^2} &= \lambda_n \bar{\phi}_n(x) \\ \bar{\phi}_n(-L_0) = \bar{\phi}_n(L_0), \qquad \frac{\mathrm{d}\bar{\phi}_n}{\mathrm{d}x}(-L_0) &= \frac{\mathrm{d}\bar{\phi}_n}{\mathrm{d}x}(L_0) \end{aligned} \tag{7}$$

yields the following solution for the eigenvalues, λ_n, and the eigenfunctions, $\bar{\phi}_n(x)$:

$$\begin{aligned} \lambda_n &= -\nu k^2 n^2, \qquad n = 0, 1, ..., \\ \phi_n(x) &= c_n \sin(knx), \quad n = 1, 2, ..., \\ \psi_n(x) &= c_n \cos(knx), \quad n = 0, 1, ..., \end{aligned} \tag{8}$$

where $\phi_n(x)$ and $\psi_n(x)$ are the two eigenfunctions corresponding to the same nonzero eigenvalue λ_n, $n \geq 1$, with a multiplicity of 2, $k = \pi/L_0$ is used to satisfy the PBCs, and c_n is introduced for the purpose of normalization with the values of $c_0 = 1/(2L_0)^{1/2}$ and $c_n = 1/(L_0)^{1/2}$, $n = 1, 2, 3, ...$ The solution of eq 3 is expanded into an infinite series in terms of the eigenfunctions of the operator of eq 7 as follows:

$$h(x,t) = \sum_{n=1}^{\infty} \alpha_n(t)\phi_n(x) + \sum_{n=0}^{\infty} \beta_n(t)\psi_n(x) \tag{9}$$

Substituting the above expansion for the solution, $h(x, t)$, into eq 3 and taking the inner product with the adjoint eigenfunctions, the following system of infinite stochastic ordinary differential equations (ODEs) is obtained:

$$\begin{aligned} \frac{\mathrm{d}\alpha_n}{\mathrm{d}t} &= \lambda_n \alpha_n + \xi_\alpha^n(t), \quad n = 1, 2, ..., \infty \\ \frac{\mathrm{d}\beta_n}{\mathrm{d}t} &= \lambda_n \beta_n + \xi_\beta{}^n(t), \quad n = 0, 1, ..., \infty \end{aligned} \tag{10}$$

where $\xi_\alpha{}^n = \int_{-L_0}^{L_0} \xi(x,t)\phi_n(x)\,\mathrm{d}x$ and $\xi_\beta{}^n = \int_{-L_0}^{L_0} \xi(x,t)\psi_n(x)\,\mathrm{d}x$ is the projection of the noise $\xi(x, t)$ in the nth ODE. We note that $\xi_\alpha{}^n$ and $\xi_\beta{}^n$, $n = 0, 1, ...$, are independent Gaussian white noise terms. Due to the linearity of the stochastic ODE system of eq 10, the system state, α_n or β_n, is independent from any other state. Therefore, the analytical solution of the state variance can be directly obtained from a direct computation as follows:

$$\begin{aligned} \langle \alpha_n{}^2(t) \rangle &= -\frac{\sigma^2}{2\lambda_n} + \left(\langle \alpha_n{}^2(t_0) \rangle + \frac{\sigma^2}{2\lambda_n} \right) e^{2\lambda_n (t - t_0)}, \quad n = 1, 2, ..., \infty \\ \langle \beta_n{}^2(t) \rangle &= -\frac{\sigma^2}{2\lambda_n} + \left(\langle \beta_n{}^2(t_0) \rangle + \frac{\sigma^2}{2\lambda_n} \right) e^{2\lambda_n (t - t_0)}, \quad n = 1, 2, ..., \infty \end{aligned} \tag{11}$$

where only expressions of the nonzeroth state variance are provided, since the zeroth state does not contribute to the mean slope square due to the spatially invariant zeroth eigenfunction.

Specifically, the expression of the steady-state value of the state variance can be obtained at the infinite-time limit as follows:

$$\langle \alpha_n{}^2 \rangle_{\mathrm{ss}} = \langle \beta_n{}^2 \rangle_{\mathrm{ss}} = -\frac{\sigma^2}{2\lambda_n} = \frac{\sigma^2}{2\nu k^2 n^2} = \frac{\sigma^2 L_0{}^2}{2\nu \pi^2 n^2}, \quad n = 1, 2, ..., \infty \tag{12}$$

Similar to the discrete lattice definition of eq 2, the continuum form of the rms slope is defined as follows:

$$m(t) = \left\{ \frac{1}{2L_0} \int_{-L_0}^{L_0} \left[\frac{\partial h}{\partial x}(x,t) \right]^2 \mathrm{d}x \right\}^{1/2} \tag{13}$$

Substituting the infinite-series expansion of $h(x, t)$ of eq 9 into 13, the expected mean slope square, $\langle m^2(t) \rangle$, can be rewritten as follows:

$$\begin{aligned} \langle m^2(t) \rangle &= \left\langle \frac{1}{2L_0} \int_{-L_0}^{L_0} \left[\frac{\partial h}{\partial x}(x,t) \right]^2 dx \right\rangle \\ &= \frac{1}{2L_0} \left\langle \int_{-L_0}^{L_0} \left[\sum_{n=1}^{\infty} \alpha_n(t) \frac{\partial \phi_n}{\partial x}(x) + \sum_{n=0}^{\infty} \beta_n(t) \frac{\partial \psi_n}{\partial x}(x) \right]^2 \mathrm{d}x \right\rangle \\ &= \frac{1}{2L_0} \left\langle \int_{-L_0}^{L_0} \left[\sum_{n=1}^{\infty} \alpha_n(t) kn \psi_n(x) - \sum_{n=1}^{\infty} \beta_n(t) kn \phi_n(x) \right]^2 \mathrm{d}x \right\rangle \\ &= \frac{1}{2L_0} \left\langle \sum_{n=1}^{\infty} k^2 n^2 \alpha_n{}^2(t) + \sum_{n=1}^{\infty} k^2 n^2 \beta_n{}^2(t) \right\rangle \\ &= \frac{1}{2L_0} \sum_{n=1}^{\infty} k^2 n^2 \langle \alpha_n{}^2(t) \rangle + \frac{1}{2L_0} \sum_{n=1}^{\infty} k^2 n^2 \langle \beta_n{}^2(t) \rangle \end{aligned} \tag{14}$$

Equation 14 provides a direct link between the state variance of the infinite stochastic ODEs of eq 10 and the expected mean slope square of the surface height profile. The steady-state value of the expected mean slope square, $\langle m^2 \rangle_{\mathrm{ss}}$, can be obtained as $t \rightarrow \infty$. By substituting the steady-state variances of eq 12 and the expressions of the eigenvalues of eq 8, the analytical form of $\langle m^2 \rangle_{\mathrm{ss}}$ is as follows:

$$\begin{aligned} \langle m^2 \rangle_{\mathrm{ss}} &= \frac{1}{2L_0} \sum_{n=1}^{\infty} k^2 n^2 \langle \alpha_n{}^2 \rangle_{\mathrm{ss}} + \frac{1}{2L_0} \sum_{n=1}^{\infty} k^2 n^2 \langle \beta_n{}^2 \rangle_{\mathrm{ss}} \\ &= -2 \frac{1}{2L_0} \sum_{n=1}^{\infty} k^2 n^2 \frac{\sigma^2}{2\lambda_n} = \frac{1}{2L_0} \sum_{n=1}^{\infty} k^2 n^2 \frac{\sigma^2}{2\nu k^2 n^2} \\ &= \frac{1}{L_0} \sum_{n=1}^{\infty} \frac{\sigma^2}{2\nu} = \frac{\sigma^2}{2\nu L_0} + \frac{\sigma^2}{2\nu L_0} + \frac{\sigma^2}{2\nu L_0} + ... \end{aligned} \tag{15}$$

From eq 15, it can be seen that each state contributes an equal finite part, $\sigma^2/(2\nu L_0)$, to the steady-state value of the expected mean slope square, $\langle m^2\rangle_{ss}$. Since the stochastic ODE system of eq 10 has infinite number of states, the steady-state value of the expected mean slope square has an infinite value. It can be also seen that $\langle m^2\rangle_{ss}$ has a reciprocal dependence on the domain size, L_0.

4.2. Discretization Analysis. In the previous section, the analytical derivation from the EW equation in a continuum domain results in an infinite steady-state value and a reciprocal domain-size dependence of the expected mean slope square. This behavior is different from the one obtained from the kMC simulations of the lattice model, which leads to a finite steady-state value and a weak lattice-size dependence of the expected mean slope square. This difference does not mean that the EW equation cannot be used to describe the evolution of the surface height profile and of the rms slope. The infinite value of the expected mean slope square from the EW equation is due to the infinitesimal discretization intervals in the continuum domain. The same behavior of rms slope can be obtained from the EW equation under a suitable finite-difference discretization of the continuum surface height profile.

Specifically, a spatial discretization is introduced to the continuum domain, $[-L_0, L_0]$. This spatial discretization contains L evenly distributed nodes, where L corresponds to the lattice size of the kMC models and is also referred to here as lattice size. The spatial coordinates of the discretization nodes can be obtained as follows:

$$x_i = x_1 + (i - 1)\Delta x, \qquad i = 2, 3, ..., L \tag{16}$$

where $x_1 \in [-L_0, -L_0 + \Delta x)$ denotes the coordinate of the first node and $\Delta x = 2L_0/L$ is the interval between two adjacent nodes. The range of x_1 indicates a freedom of choosing the discretization, as long as the continuum domain is evenly discretized. The choice of the specific discretization does not affect the analysis and the numerical results.

With the finite-dimensional discretization, the mean slope square of a discrete surface height profile can be computed in a similar fashion as in the kMC simulations:

$$m^2 = \frac{1}{L}\sum_{i=1}^{L}\left(\frac{h_{i+1} - h_i}{\Delta x}\right)^2 \tag{17}$$

where h_i denotes the surface height at the ith node and $h_i(t) = h(x_i, t)$.

By substituting the definition of mean slope square of eq 17 and the expansion of the surface height profile of eq 9, the expected mean slope square can be manipulated as follows (the zeroth state does not contribute to the expected mean slope square because $\phi_0(x)$ is a constant function):

$$\begin{aligned}\langle m^2(t)\rangle &= \left\langle \frac{1}{L\Delta^2 x}\sum_{i=1}^{L}\Big[\sum_{n=1}^{\infty}\alpha_n(t)\Delta\phi_n(x_i) + \sum_{n=1}^{\infty}\beta_n(t)\Delta\psi_n(x_i)\Big]^2\right\rangle \\ &= \frac{1}{L\Delta^2 x}\sum_{i=1}^{L}\Big[\sum_{n=1}^{\infty}\langle\alpha_n^2(t)\rangle\Delta^2\phi_n(x_i) + \sum_{n=1}^{\infty}\langle\beta_n^2(t)\rangle\Delta^2\psi_n(x_i)\Big] \\ &= \sum_{n=1}^{\infty}\left[\frac{1}{L\Delta^2 x}\sum_{i=1}^{L}\Delta^2\phi_n(x_i)\right]\langle\alpha_n^2(t)\rangle + \\ &\qquad \sum_{n=1}^{\infty}\left[\frac{1}{L\Delta^2 x}\sum_{i=1}^{L}\Delta^2\psi_n(x_i)\right]\langle\beta_n^2(t)\rangle\end{aligned} \tag{18}$$

where $\Delta f(x_i) = f(x_{i+1}) - f(x_i)$ and $\Delta^2 f(x_i) = [\Delta f(x_i)]^2$. We note that, due to the independence of the system states, $\langle\alpha_{n_1}(t)\alpha_{n_2}(t)\rangle = \langle\beta_{n_1}(t)\beta_{n_2}(t)\rangle = 0$, for $n_1 \neq n_2$, and $\langle\alpha_{n_1}(t)\beta_{n_2}(t)\rangle = 0$, for any n_1 and n_2, $n_1 = 1, 2, ...$, and $n_2 = 1, 2, ...$

The expression of the expected mean slope square of eq 18 can be further simplified into the following form:

$$\langle m^2(t)\rangle = \sum_{n=1}^{\infty}K_n^{\alpha}\langle\alpha_n^2(t)\rangle + \sum_{n=1}^{\infty}K_n^{\beta}\langle\beta_n^2(t)\rangle \tag{19}$$

where K_n^{α} and K_n^{β} denote the coefficients of the state variance and have the following analytical form:

$$K_n^{\alpha} = K_n^{\beta} = \frac{4}{L\Delta^3 x}\sin^2\left(\frac{n\pi}{L}\right) \tag{20}$$

With the solution expression of the expected mean slope square of eq 19, it can be proved that the expected mean slope square from finite discretization has a finite steady-state value, which is consistent with the kMC simulation results of the lattice models. Derivation of the analytical form of K_n of eq 20 and proof of the finite steady-state value of the expected mean slope square can be found in the Appendix at the end of this manuscript.

Remark 3. *We note that there is no connection, established from a physical (first principles) point of view, between the metric m computed on the basis of the surface profile of the kMC simulations and the derivative of the surface height of the EW equation. The reason we consider the EW equation and present profiles of the metric m on the basis of the surface height profile of the EW equation is because the EW equation with appropriately fitted parameters to kMC data can be used to approximately predict the evolution of m of the kMC simulation with finite lattice size, and thus, it can be incorporated in model-based feedback control schemes to make predictions of the evolution of the mean slope m. In previous work, we have demonstrated that this approach leads to a controller design that works well for simultaneous regulation of surface slope and roughness.*[29] *We also note that the EW equation is a reasonable model for the thin-film growth process because it captures the balance between random adsorption and thermal migration (diffusion) and predicts certain scaling properties (lattice-size dependence of roughness) obtained from kMC simulation of the deposition processes under consideration. Furthermore, EW equation-based control can be applied to an actual thin-film manufacturing process when the EW equation parameters are computed on the basis of experimental data.*

4.3. Numerical Results of Discretized Solution. In this subsection, the numerical simulations of the EW equation are used to verify the solution of the expected mean slope square derived in the previous subsection under the finite discretization. The numerical results are also compared to demonstrate their consistency with the kMC simulation results of the lattice models.

To carry out the numerical calculations of the mean slope square under the finite difference discretization, numerical simulations are first carried out to compute solutions of the EW equation, i.e., the solutions of surface height profile. The numerical solutions of the EW equation can be obtained from a high-order approximation of the infinite ODE system of eq 10. Due to the decoupled nature of the linear ODE system, the solution of each state is a stochastic process, which is independent from the other states. Since the ODE system contains an infinite number of states and results in an infinite computational time for the solution, a reduced-order system with a sufficiently large number of modes (the number of modes is 100 times the number of discretization nodes) is used as an

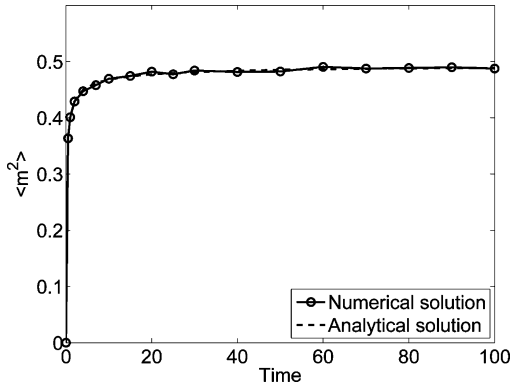

Figure 17. Profile of the expected mean slope square from the discretized solution of the EW equation from numerical simulations (solid line) and from analytical solutions (dashed line); $\Delta x = 1$, $L = 100$.

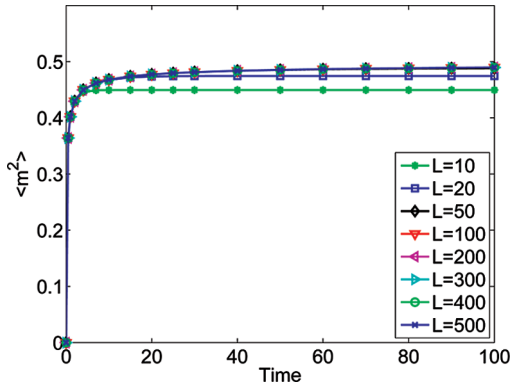

Figure 18. Profile of the expected mean slope square from the discretized solution of the EW equation with different domain sizes; $\Delta x = 1$.

approximation of the infinite-order system. The solution of the surface height profile is then sampled at discrete positions to obtain a discrete surface height profile. The sampled positions are the coordinates of the discretization nodes defined in eq 16, which are evenly distributed in the spatial domain. Finally, the expected rms slope and the expected mean slope square can be computed from the discrete surface height profile. Since the numerical solutions are stochastic realizations of the analytical solution, multiple independent numerical solutions are obtained to calculate the expected mean slope square.

Figure 17 shows the profile of the expected mean slope square of the discretized solution of the EW equation. In Figure 17, the profile from numerical solutions is compared with the profile from the analytical solution that is derived previously in section 4.2. The analytical solution is obtained from the same high-order approximation as the numerical solutions. The values of parameters of the EW equation are $\nu = 1$ and $\sigma^2 = 1$ for all simulations in this subsection. The domain size is $L_0 = 50$ and the discretization interval is $\Delta x = 1$. Thus, the lattice size is $L = 100$. From Figure 17, it can be seen that the derived analytical solution of the expected mean slope square fits very well with numerical solutions of the EW equation. Therefore, the analytical solution can be used to predict the mean slope square evolution.

Figure 18 shows the profiles of the expected mean slope square obtained from the EW equation for different domain sizes ranging from $L_0 = 5$ to $L_0 = 250$. We note that the lattice size changes simultaneously and proportionally with the domain size. As a result, the same discretization interval, Δx, is preserved, which corresponds to the size of particles in the lattice model. Therefore, the number of discretization nodes, which is also

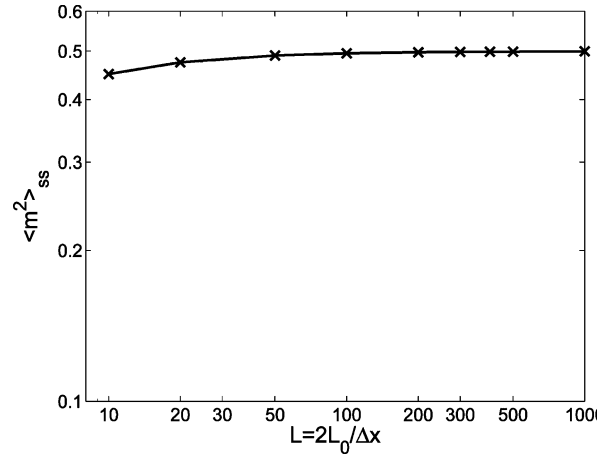

Figure 19. Dependence of the steady-state value of the expected mean slope square obtained from the discretized solution of the EW equation, on the lattice size, L; $\Delta x = 1$.

denoted by L, ranges from $L = 10$ to 500. In Figure 18, the expected mean slope square profiles evolve similarly to the profiles from the discrete lattice kMC model shown in Figure 5.

The lattice-size dependence of the expected mean slope square can be obtained from the analytical solution for different domain sizes and correspondingly different lattice sizes. Figure 19 shows the lattice-size dependence of the steady-state value of the expected mean slope square. From Figure 19, it can be seen that the steady-state value of the expected mean slope square has a weak dependence on lattice size, especially at large lattice sizes. We note that this lattice-size dependence is obtained on the basis of the fixed discretization interval, Δx.

From Figures 18 and 19, the same behavior is observed from the discretized solution of the EW equation as the ones from the kMC simulations of the lattice model, i.e., a finite steady-state value and a weak lattice-size dependence of the steady-state value of the expected mean slope square. The consistency between the discretized solution of the EW equation and of the kMC simulations supports the choice of the EW equation as the dynamic model for the surface height profile evolution in the deposition processes under consideration.

The discretization can also explain the infinite steady-state value of the mean slope square of the EW equation in the continuum domain of eq 15. The infinite value originates from the infinitesimal discretization intervals in the continuum case, which can be observed from the analytical results of the discretized solutions of the EW equation with decreasing discretization intervals. The domain size is kept constant, and thus, the lattice size is proportional to $1/\Delta x$. Figure 20 shows the dependence of the steady-state value of the expected mean slope square from the discretized solution of the EW equation for different discretization intervals. It can be clearly seen that as the discretization interval decreases to zero, the steady-state means slope square increases and the dependence of $\langle m^2 \rangle_{ss}$ on $1/\Delta x$ is linear. The same behavior of the steady-state value of $\langle m^2 \rangle_{ss}$ can be obtained from the kMC simulations of both deposition processes; see Figure 21 for the random deposition with surface relaxation process and Figure 22 for the porous thin-film deposition process. We note that the counterpart of the discretization interval in the kMC models of the deposition processes is the sampling interval, i.e., the distance between the points of the surface height profile that are used to calculate the surface slope and is denoted as Δx as well. Thus, the sampling intervals of the deposition process have a minimum

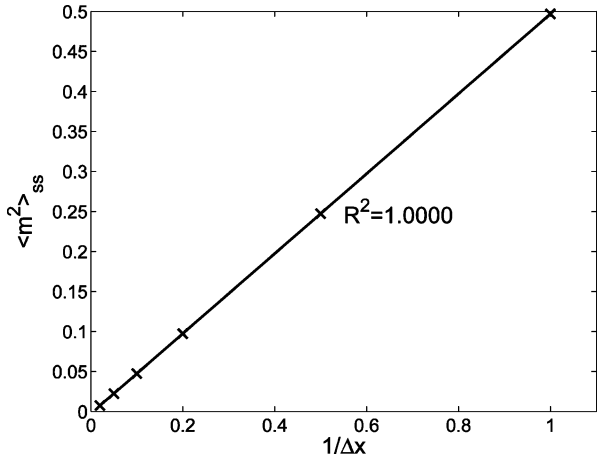

Figure 20. Dependence of the steady-state value of the expected mean slope square obtained from the discretized solution of the EW equation on the discretization interval; $L_0 = 100$.

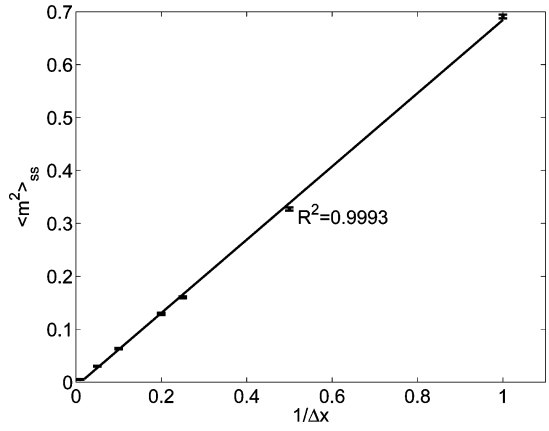

Figure 21. Dependence of the steady-state value of the expected mean slope square with error bars on the sampling interval; random deposition with surface relaxation process with $W = 1$ layer/s and $L = 200$.

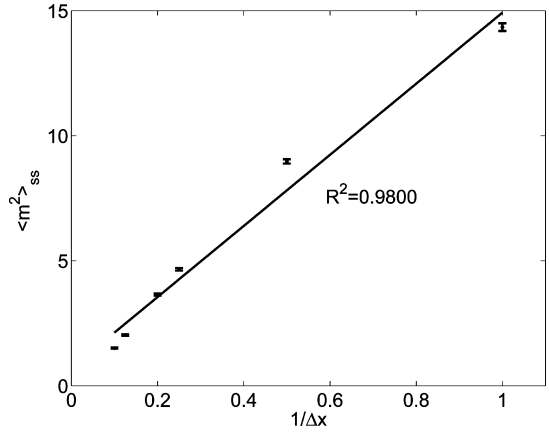

Figure 22. Dependence of the steady-state value of the expected mean slope square with error bars on the sampling interval; porous thin-film deposition process with $W = 1$ layer/s, $T = 300$ K, and $L = 200$.

value of one; smaller sampling intervals are not possible due to the lattice size limitation, which is different from the EW equation in the continuum domain where Δx can be chosen at will.

Remark 4. *The dependence of the steady-state value of the expected mean slope square on the sampling interval, Δx, in the porous thin-film deposition process is linear for large Δx, as shown in Figure 22, which is similar to the linear dependence observed in the random deposition with surface relaxation process and in the EW equation shown in Figures 20 and 21, respectively. However, at the discrete limit, $\Delta x = 1$, the dependence on Δx in the porous film process has a notable deviation from the linear dependence. This deviation is due to the triangular lattice structure and the porosity allowed in the thin-film deposition process. To calculate the surface height profile of the deposition process taking place on a triangular lattice, 2L points are needed for the surface height positions, i.e., h_1, h_2, ..., h_{2L}. However, since there are only L lattice sites in a row (in the lateral direction), the 2L surface heights are not fully independent. Instead, these heights are correlated to their neighboring heights via the structure of the triangular lattice. This correlation reduces the irregularity of the surface and results in close steady-state values of expected mean slope square for $\Delta x = 1$ and $\Delta x = 2$ in the porous thin-film deposition process.*

Remark 5. *This work mainly focuses on the dynamic behavior of the surface slope of thin-film growth processes that can be described by the EW equation. A potential application of this work is to improve light trapping efficiency of thin-film solar cells by simultaneously regulating surface roughness and slope of the thin-films during the manufacturing process. To achieve the control objectives, macroscopic variables including the substrate temperature and the deposition rate or the inlet concentration of the deposition reactor may be chosen as the manipulated variable(s). Model predictive control can be designed based on state feedback or measurements by formulating an optimization problem that minimizes the deviations of the surface roughness square and of the mean slope square from desired set-point values that optimize light trapping. With respect to measurement of surface mean slope, atomic force microscopy measurements of the film surface can be used to obtain surface height profiles up to atomic dimensions and from this compute the local surface mean slope variable. Aggregate surface height can also be computed from the atomic force microscopy measurements of the film surface to compute surface slope of aggregate surface height that is relevant to visible light trapping of thin-film solar cells. The detailed development of this controller design approach has been the subject of another work.*

5. Conclusion

In this work, the dynamic behavior and lattice-size dependence of the surface root-mean-square slope were investigated in two thin-film deposition processes that involve thermal balance between film growth and surface relaxation. Specifically, two different deposition processes taking place on square and triangular lattices were introduced and used to investigate the dynamics and lattice-size dependence of surface root-mean-square slope. The simulation results indicate that the expected mean slope square reaches quickly a steady-state value and exhibits a very weak dependence with respect to lattice size variation. The simulation findings were corroborated by an analysis of appropriate finite-difference discretizations of surface height profiles computed by an EW-type partial differential equation that can be used to describe the dynamics of surface height profile in the deposition processes under consideration.

Acknowledgment

The authors are grateful to the Intel Higher Education Program, which provided the Linux cluster used in the simulations. Financial support from NSF, CBET-0652131, is gratefully acknowledged.

Appendix

Derivation of the state coefficients, K_n^{α} and K_n^{β}, of eq 20, can be found in the following steps. Since K_n^{α} and K_n^{β} have the same value and the derivation steps are similar, we only show the derivation of K_n^{α} from $\phi_n(x)$. The same value of K_n^{β} can be obtained from $\psi_n(x)$ via a similar derivation procedure.

From eq 18, the state coefficient, K_n^{α} has the following form:

$$K_n^{\alpha} = \frac{1}{L\Delta^2 x}\sum_{i=1}^{L}\Delta^2\bar{\phi}_n(x_i) \tag{21}$$

By substituting the expression of the eigenfunction ϕ_n of eq 8 into eq 21, the expression of K_n^{α} can be rewritten as follows:

$$\begin{aligned} K_n^{\alpha} &= \frac{1}{L\Delta^2 x}\sum_{i=1}^{L}[\phi_n(x_{i+1}) - \phi_n(x_i)]^2 \\ &= \frac{1}{L\Delta^2 x}\sum_{i=1}^{L}[c_n\sin(knx_{i+1}) - c_n\sin(knx_i)]^2 \\ &= \frac{1}{L\Delta^2 x}\sum_{i=1}^{L}\left\{2c_n\cos\left[\frac{kn}{2}[x_{i+1}+x_i)\right]\sin\left[\frac{kn}{2}[x_{i+1}-x_i)\right]\right\}^2 \\ &= \frac{4}{L\Delta^2 x}\sum_{i=1}^{L}{c_n}^2\cos^2\left[\frac{kn}{2}(x_{i+1}+x_i)\right]\sin^2\left(\frac{kn\Delta x}{2}\right) \\ &= \frac{4}{L\Delta^2 x}\sum_{i=1}^{L}{c_n}^2\cos^2\left[\frac{kn}{2}(x_{i+1}+x_i)\right]\sin^2\left(\frac{kn\Delta x}{2}\right) \end{aligned} \tag{22}$$

Equation 22 can be further simplified into the following form by substituting the expressions of $\Delta x = 2L_0/L$, $k = \pi/L_0$, $c_n = 1/(L_0)^{(1/2)}$ for $n \geq 1$), and the expression of x_i of eq 16:

$$\begin{aligned} K_n^{\alpha} &= \frac{4}{L\Delta^2 x}\sum_{i=1}^{L}\frac{1}{L_0}\cos^2\left[knx_1 - \frac{n\pi}{L} + i\frac{2n\pi}{L}\right]\sin^2\left(\frac{n\pi}{L}\right) \\ &= \frac{8}{L^2\Delta x^3}\sum_{i=1}^{L}\cos^2\left[knx_1 - \frac{n\pi}{L} + i\frac{2n\pi}{L}\right]\sin^2\left(\frac{n\pi}{L}\right) \end{aligned} \tag{23}$$

The following result is used to simplify the expression of K_n^{α} further:

Result 1

If (1) $\theta_0 \in R$, (2) $n_1 \geq 1$ and $n_2 \geq 2$ are integers, and (3) $\theta = 2n_1\pi/n_2$, then it can be derived that

$$\sum_{i=1}^{n_2}\cos^2(\theta_0 + i\theta) = \begin{cases} n_2\cos^2\theta_0, & n_2 = 2,4,6,..., \text{ and } n_1 = \frac{1}{2}n_2, n_2, \frac{3}{2}n_2, ... \\ \frac{n_2}{2}, & \text{otherwise} \end{cases} \tag{24}$$

Proof of Result 1

If n_2 is an even integer and $n_1 = n_2/2$, n_2, $3n_2/2$, ..., i.e., $\theta = 2n_1\pi/n_2 = \pi, 2\pi, ...$, the sum of the series of cosine square can be directly obtained as follows:

$$\sum_{i=1}^{n_2}\cos^2(\theta_0 + i\theta) = \sum_{i=1}^{n_2}\cos^2\theta_0 = n_2\cos^2\theta_0 \tag{25}$$

Otherwise, the sum of the series of cosine square can be rewritten in the following form:

$$\begin{aligned} \sum_{i=1}^{n_2}\cos^2(\theta_0 + i\theta) &= \sum_{i=1}^{n_2}\left[\frac{1}{2} + \frac{1}{2}\cos(2\theta_0 + 2i\theta)\right] = \frac{n_2}{2} + \\ &\frac{1}{2}\sum_{i=1}^{n_2}\mathrm{Re}(e^{j(2\theta_0+2i\theta)}) = \frac{n_2}{2} + \frac{1}{2}\mathrm{Re}(e^{j2\theta_0}\sum_{i=1}^{n_2}e^{j2i\theta}) \end{aligned} \tag{26}$$

where j denotes the imaginary unit, and $\mathrm{Re}(\cdot)$ denote the real part of a complex number. The sum of the geometric series can be further simplified as follows:

$$\begin{aligned} \sum_{i=1}^{n_2}\cos^2(\theta_0 + i\theta) &= \frac{n_2}{2} + \frac{1}{2}\mathrm{Re}\left(e^{j2\theta_0}e^{j2\theta}\frac{1 - e^{j2n_2\theta}}{1 - e^{j2\theta}}\right) = \frac{n_2}{2} + \frac{1}{2}\mathrm{Re} \\ &\left(e^{j2\theta_0}e^{j2\theta}\frac{1 - e^{j4n_1\pi}}{1 - e^{j2\theta}}\right) = \frac{n_2}{2} + \frac{1}{2}\mathrm{Re}(0) = \frac{n_2}{2} \end{aligned} \tag{27}$$

since the denominator $1 - \exp(j2\theta) = 1 - \exp(j2\pi(2n_1/n_2)) \neq 0$.

By using result 1, the expression of K_n can be obtained as follows:

$$K_n^{\alpha} = \begin{cases} \frac{8}{L\Delta x^3}\sin^2\left(\frac{n\pi}{L}\right)\cos^2\left(knx_1 - \frac{n\pi}{L}\right), & n = \frac{1}{2}L, L, \frac{3}{2}L, ... \\ \frac{4}{L\Delta x^3}\sin^2\left(\frac{n\pi}{L}\right), & \text{otherwise} \end{cases} \tag{28}$$

Equation 28 indicates that for certain values of n ($n = (1/2)L, L, (3/2)L, ...$), the value of K_n depends on the choice of the spatial coordinate of the first discretization node, x_1, which can be any value from $-L_0$ to $-L_0 + \Delta x$. Thus, a general expression of K_n^{α} is desired and can be obtained by averaging over all possible $x_1 \in [-L_0, -L_0 + \Delta x)$ as follows:

$$K_n^{\alpha} = \frac{1}{\Delta x}\int_{-L_0}^{-L_0+\Delta x}K_n(x_1)\,dx_1 = \frac{4}{L\Delta x^3}\sin^2\frac{n\pi}{L}, \qquad n \geq 1 \tag{29}$$

Similarly, K_n^{β} can be obtained with the same value as K_n^{α}.

After the expressions of K_n^{α} and K_n^{β} are obtained, the steady-state value of the expected mean slope square can be computed by taking the infinite-time limit of eq 19 and substituting the steady-state variance of eq 12 as follows:

$$\begin{aligned} \langle m^2\rangle_{ss} &= \sum_{n=1}^{\infty}K_n^{\alpha}\langle{\alpha_n}^2\rangle_{ss} + \sum_{n=1}^{\infty}K_n^{\beta}\langle{\beta_n}^2\rangle_{ss} \\ &= \sum_{n=1}^{\infty}2\frac{4}{L\Delta x^3}\frac{\sigma^2L^2}{2\nu\pi^2n^2}\sin^2\left(\frac{n\pi}{L}\right) \\ &= \frac{4L\sigma^2}{\nu\pi^2\Delta x^3}\sum_{n=1}^{\infty}\frac{1}{n^2}\sin^2\left(\frac{n\pi}{L}\right) \end{aligned} \tag{30}$$

Since $0 \leq \sin^2(n\pi/L) \leq 1$, it can be shown that the steady-state expected mean slope square has a finite upper bound as follows:

$$\langle m^2\rangle_{ss} \leq \frac{4L\sigma^2}{\nu\pi^2\Delta x^3}\sum_{n=1}^{\infty}\frac{1}{n^2} = \frac{4L\sigma^2}{\nu\pi^2\Delta x^3}\frac{\pi^2}{6} = \frac{2L\sigma^2}{\nu\Delta x^3} \tag{31}$$

Therefore, the expected mean slope square has a finite value at the steady state.

Literature Cited

(1) Shi, Z.; Green, M. A. Survey of material options and issues for thin-film silicon solar cells. *Prog. Photovoltaics Res. Appl.* **1998**, *6*, 247–257.

(2) Krč, J.; Smole, F.; Topič, M. Analysis of light scattering in amorphous Si:H solar cells by a one-dimensional semi-coherent optical model. *Prog. Photovoltaics Res. Appl.* **2003**, *11*, 15–26.

(3) Müller, J.; Rech, B.; Springer, J.; Vanecek, M. TCO and light trapping in silicon thin-film solar cells. *Sol. Energy* **2004**, *77*, 917–930.

(4) Vorburger, T. V.; Marx, E.; Lettieri, T. R. Regimes of surface roughness measurable with light scattering. *Appl. Opt.* **1993**, *32*, 3401–3408.

(5) Christofides, P. D.; Armaou, A.; Lou, Y.; Varshney, A. *Control and Optimization of Multiscale Process Systems*; Birkhäuser: Boston, 2008.

(6) Levine, S. W.; Clancy, P. A simple model for the growth of polycrystalline Si using the kinetic Monte Carlo simulation. *Model. Simul. Mater. Sci. Eng.* **2000**, *8*, 751–762.

(7) Levine, S. W.; Engstrom, J. R.; Clancy, P. A kinetic Monte Carlo study of the growth of Si on Si(100) at varying angles of incident deposition. *Surf. Sci.* **1998**, *401*, 112–123.

(8) Zhang, P.; Zheng, X.; Wu, S.; Liu, J.; He, D. Kinetic Monte Carlo simulation of Cu thin-film growth. *Vacuum* **2004**, *72*, 405–410.

(9) Wang, L.; Clancy, P. Kinetic Monte Carlo simulation of the growth of polycrystalline Cu films. *Surf. Sci.* **2001**, *473*, 25–38.

(10) Hu, G.; Huang, J.; Orkoulas, G.; Christofides, P. D. Investigation of Film Surface Roughness and Porosity Dependence on Lattice Size in a Porous thin-film Deposition Process. *Phys. Rev. E* **2009**, *80*, 041122.

(11) Lou, Y.; Christofides, P. D. Estimation and Control of Surface Roughness in thin-film Growth Using Kinetic Monte-Carlo Models. *Chem. Eng. Sci.* **2003**, *58*, 3115–3129.

(12) Lou, Y.; Christofides, P. D. Feedback Control of Growth Rate and Surface Roughness in thin-film Growth. *AIChE J.* **2003**, *49*, 2099–2113.

(13) Edwards, S. F.; Wilkinson, D. R. The surface statistics of a granular aggregate. *Proc. R. Soc. London, Ser. A* **1982**, *381*, 17–31.

(14) Kardar, M. Roughness and ordering of growing films. *Physica A* **2000**, *281*, 295–310.

(15) Haselwandter, C. A.; Vvedensky, D. D. Stochastic equation for the morphological evolution of heteroepitaxial thin-films. *Phys. Rev. B* **2006**, *74*, 121408.

(16) Haselwandter, C. A.; Vvedensky, D. D. Renormalization of stochastic lattice models: Basic formulation. *Phys. Rev. E* **2007**, *76*, 041115.

(17) Haselwandter, C. A.; Vvedensky, D. D. Renormalization of stochastic lattice models: Epitaxial surfaces. *Phys. Rev. E* **2008**, *77*, 061129.

(18) Hu, G.; Lou, Y.; Christofides, P. D. Dynamic Output Feedback Covariance Control of Stochastic Dissipative Partial Differential Equations. *Chem. Eng. Sci.* **2008**, *63*, 4531–4542.

(19) Christofides, P. D.; Armaou, A. Control and optimization of multiscale process systems. *Comp. Chem. Eng.* **2006**, *30*, 1670−1686.

(20) Hu, G.; Orkoulas, G.; Christofides, P. D. Modeling and Control of Film Porosity in thin-film Deposition. *Chem. Eng. Sci.* **2009**, *64*, 3668–3682.

(21) Hu, G.; Orkoulas, G.; Christofides, P. D. Regulation of Film Thickness, Surface Roughness and Porosity in thin-film Growth Using Deposition Rate. *Chem. Eng. Sci.* **2009**, *64*, 3903–3913.

(22) Hu, G.; Orkoulas, G.; Christofides, P. D. Stochastic Modeling and Simultaneous Regulation of Surface Roughness and Porosity in thin-film Deposition. *Ind. Eng. Chem. Res.* **2009**, *48*, 6690–6700.

(23) Lou, Y.; Christofides, P. D. Feedback Control of Surface Roughness Using Stochastic PDEs. *AIChE J.* **2005**, *51*, 345–352.

(24) Yang, Y. G.; Johnson, R. A.; Wadley, H. N. A Monte Carlo simulation of the physical vapor deposition of nickel. *Acta Mater.* **1997**, *45*, 1455–1468.

(25) Vlachos, D. G.; Schmidt, L. D.; Aris, R. Kinetics of faceting of crystals in growth, etching, and equilibrium. *Phys. Rev. B* **1993**, *47*, 4896–4909.

(26) Barabási, A.-L.; Stanley, H. E. *Fractal Concepts in Surface Growth*; Cambridge University Press: New York, 1995.

(27) Family, F. Scaling of rough surfaces: effects of surface diffusion. *J. Phys. A: Math. Gen.* **1986**, *19*, L441–L446.

(28) Ni, D.; Christofides, P. D. Multivariable Predictive Control of thin-film Deposition Using a Stochastic PDE Model. *Ind. Eng. Chem. Res.* **2005**, *44*, 2416–2427.

(29) Zhang, X.; Hu, G.; Orkoulas, G.; Christofides, P. D. Predictive control of surface mean slope and roughness in a thin-film deposition process. *Chem. Eng. Sci.*, in press.

Received for review January 3, 2010
Revised manuscript received April 28, 2010
Accepted May 5, 2010

IE100012W